Si/SiGe Nanolithography and Si/SiGe Wires

Y. Zhuang, C. Schelling, A. Daniel, T. Roch, M. Mühlberger, F. Schäffler, G. Bauer

Institut für Halbleiter- und Festkörperphysik, Johannes Kepler Universität Linz, A-4040 Linz, Austria

S. Senz

Max-Planck-Institut für Mikrostrukturforschung, D-06120 Halle, Germany

$Si/Si_{1-x}Ge_x$ nanostructures (wires) were grown by local solid source molecular beam epitaxy using three kinds of masks: Si, SiO_2, and SiO_2/Si_3N_4. Photoluminescence measurements were performed to establish their electronic properties and to find out the most appropriate fabrication method. Their structural properties were studied by transmission electron microscopy to obtain information on the shape of cross sections, and by x-ray coplanar and grazing incidence diffraction, which yielded depth-dependent in-plane strain distribution in the wires as well as in the substrate, which was compared to results of finite element calculations.

1. Introduction

Reactive ion etching of Si/SiGe quantum wells is known to result in structures with sidewall defects, which drastically decrease their luminescence efficiency [1], [2]. Consequently, several groups have developed techniques for the direct growth of Si/SiGe quantum wells with finite lateral widths, i.e. of wires, using local solid source [3] – [5] or gas source molecular beam epitaxy (MBE) [6], [7]. In particular, by local MBE growth through shadow masks Si/SiGe wire-like structures were fabricated with lateral dimensions down to 100 nm [5]. Ge rich self-organized quantum dots down to 70nm were selectively grown into windows defined by holes in SiO_2 masks by Kim et al. [6].

We report on selectively grown Si/SiGe multilayers using three different kinds of masks: Si, SiO_2 and SiO_2/Si_3N_4. It turns out that on patterned substrates the conventional cleaning step to remove the oxide by heating the wafers up to 950 °C results in a remarkable change of the substrate surface profile indicating significant mass transport [8] – [10]. Photoluminescence was observed from wire structures for all three types of masks, however. The highest efficiency was obtained with deep etched Si masks. We investigated the structural properties of locally grown heterostructures by using transmission electron microscopy (TEM) and high resolution x-ray diffraction. With the latter technique we obtain information on the strain status of the locally grown Si/SiGe wires, their lattice relaxation and the strain status of the substrate close to the surface, induced by patterning and overgrowth. The experimental results on the lattice strain are compared with finite element calculations.

2. Experimental

2.1 Sample preparation

Periodic $Si/Si_{1-x}Ge_x$ wire structures were grown by MBE through three different kinds of shadow masks, shown schematically in Figs.1 and 2, which represent the SiO_2, the SiO_2/Si_3N_4 shadow masks, and the deep etched Si mask. In the first sample series (Fig. 1 (a)), a 105 nm thick thermal SiO_2 layer was laterally structured into wires with periods of 800 nm. In the grooves on the Si surface, $Si/Si_{1-x}Ge_x$ multilayer structures were deposited. In the second series (Fig. 1 (b)), the thermal SiO_2 layer was capped with a 150 Å Si_3N_4 layer. After reactive etching, the SiO_2 layer was selectively etched by HF to create an undercut and thus lead to a Si_3N_4 shadow mask. $Si/Si_{1-x}Ge_x$ multilayers were grown on the Si(001) substrate through this Si_3N_4 shadow mask. In the third series, the 105 nm thick thermal SiO_2 layer was laterally structured into wires with periods of 800 nm and then the Si was deep etched to about 300 nm. Holographic lithography was performed using an Ar ion laser operating at a wavelength of 458nm, the plasma etching was performed in an Oxford Plasmalab with a parallel plate reactor. For Si etching, a mixture of SF_6 with CH_4 was used, for Si_3N_4 and SiO_2, a mixture of CF_4 with H_2.

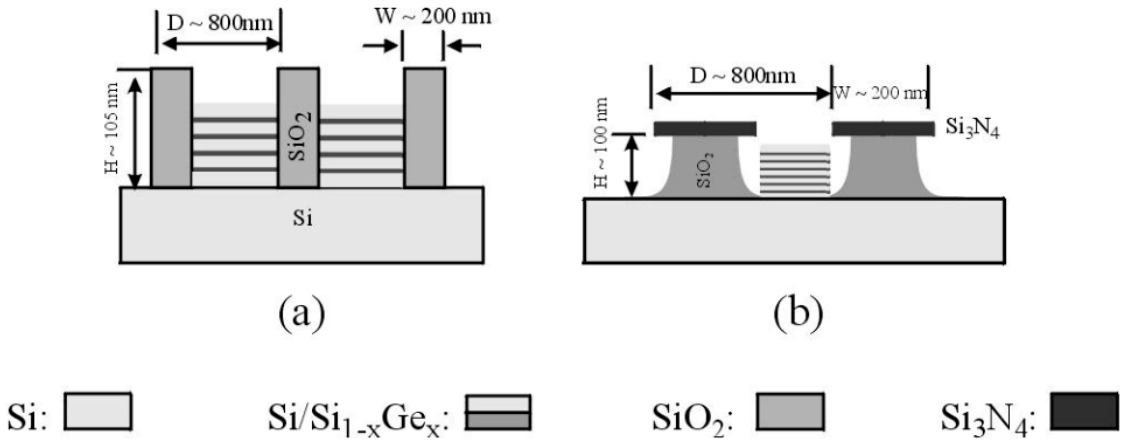

Fig. 1: Sketch of the Si/SiGe MQW wire grown through a SiO_2 and a SiO_2/Si_3N_4 shadow mask with lateral periods of about 800 nm.

2.2 Experimental results: photoluminescence

Prior to the growth of $Si/Si_{1-x}Ge_x$ MQWs on the patterned substrates, a 6 minutes thermal annealing step at 950 °C was employed to desorb the oxide layer generated during an HF free RCA cleaning procedure. From the TEM we find that this thermal-cleaning procedure leads to a significant mass transport and change of the surface profile. This mass transport is absent for a cleaning procedure involving a thermal treatment at only 650 °C. The Si substrate remains flat, and the MQW structure does not wet the etched SiO_2 wires.

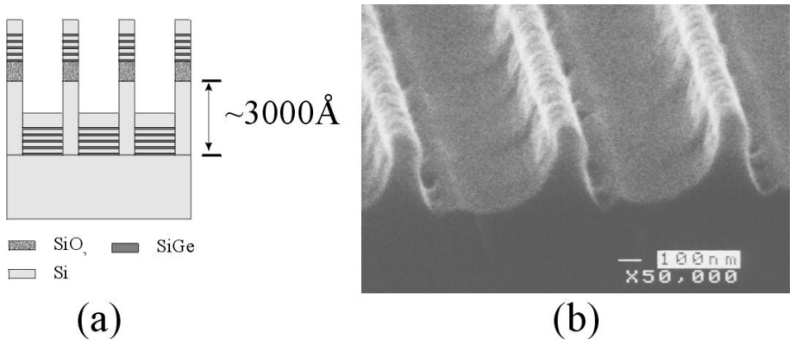

Fig. 2: (a) Sketch of the Si/SiGe MQW wires grown is deep etched Si; (b) scanning electron micrograph cross sectional view after MBW wire growth.

Photoluminescence spectra from the selectively grown $Si/Si_{1-x}Ge_x$ MQWs for the two kinds of masks shown in Fig.1 are presented in Fig.3. For these samples the conventional cleaning step at 950 °C was performed. The PL spectra were acquired at 4.2 K using an excitation laser wavelength of 488 nm, normal incidence and a power density of 0.4 W/cm^2. For the Si_3N_4 shadow mask a lift-off was performed by selective wet chemical etching. The observed $Si/Si_{1-x}Ge_x$ MQW PL lines correspond to the no-phonon line (NP), and its transverse optical phonon replica (TO). Signatures from the $Si/Si_{1-x}Ge_x$ quantum wells with finite lateral size are clearly observed for growth through both kinds of masks. It also turned out that the overall PL intensity of the wire structures is smaller for those grown between the SiO_2 wires, which exhibit high defect densities at the side wall boundaries to the oxide. Compared to such samples, a significant improvement of the luminescence efficiency (Fig. 4) is obtained for those grown into deep etched Si (Fig.2) , for which the cleaning step at 950°C was performed. The intensity from the Si/SiGe wires is higher than that from the Si substrate, which demonstrates the high PL efficiency from the wires. The FWHM of the PL lines from the wires is of the order of 10 meV, comparable to that of quantum wells. This clearly offers further possibilities for the fabrication of such high performance devices which need local epitaxial overgrowth. The lateral wire width does not yet induce any quantum confinement, this can only be observed for sizes smaller than about 40nm.

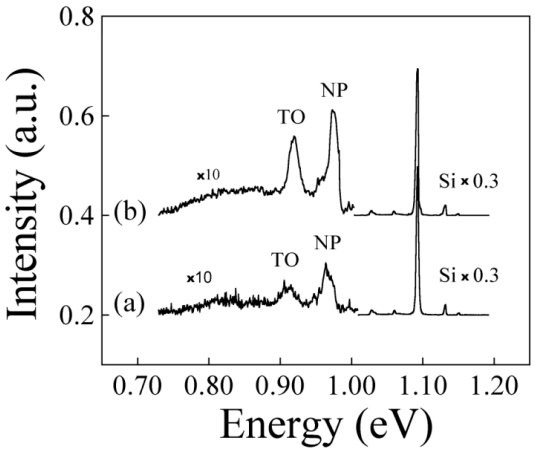

Fig. 3: PL spectra of Si/SiGe wire structure growth through the periodic SiO_2 mask (a) and through the SiO_2/Si_3N_4 mask (b).

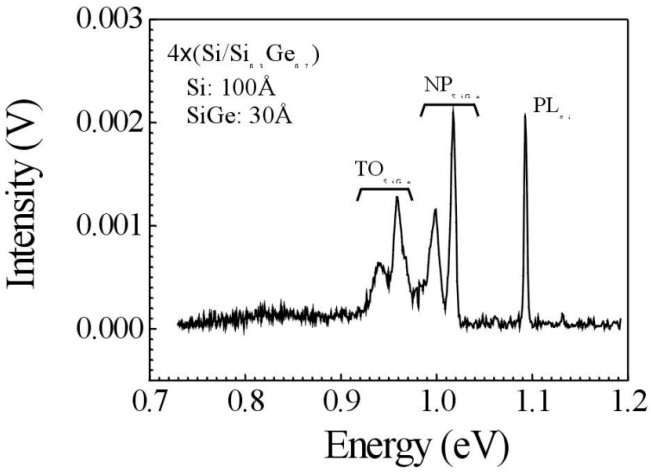

Fig. 4: PL spectra of Si/SiGe wire structure growth through the periodic SiO_2 mask in the deep etched Si wires (sample SEM shown in Fig. 2 (b)).

2.3 Strain investigations

For the strain analysis we use high angle x-ray diffraction and grazing incidence diffraction (GID) for resolving changes of the strain status with depth from the free surface and a comparison with finite element calculations. HRXRD measurements were performed for obtaining the average in-plane and vertical strain tensor components ε_{xx} and ε_{zz}, using reciprocal space maps around the (004) and the (224) reciprocal lattice points [7]. In Fig. 5, three q_x-scans (q_x denotes the x component of $q = 4\pi\sin\theta_B/\lambda$, θ_B is the Bragg angle and λ the wavelength), recorded in the vicinity of the (224) reciprocal lattice point are shown.

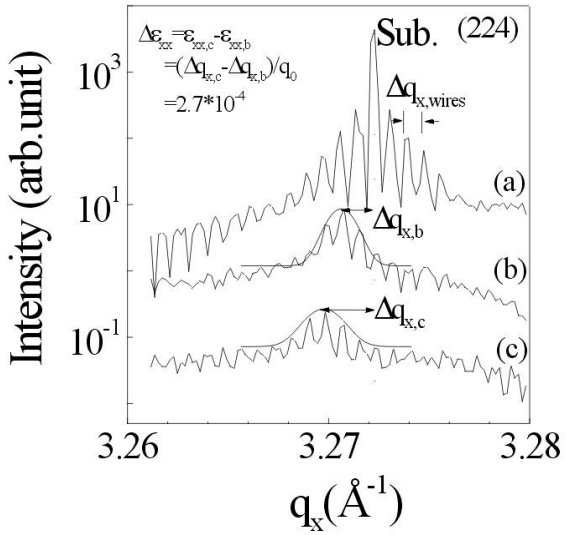

Fig. 5: X-ray diffraction of wire sample: q_x-scans in the (224) reciprocal space map across the substrate (a), the SL_0 peak (b) before removing the wire mask, and after removal of the shadow mask (c) .

Due to the orientation of the scattering vector perpendicular to the wires, several grating peaks appear, which reflect the lateral periodicity D of the wires: $D = 2\pi/\Delta q_{x,wires}$. Curve a is a scan through the Si substrate, b and c are scans through the 0^{th} order Si/SiGe superlattice peak (SL_0) corresponding to data obtained on a wire sample (Fig. 1 (b)) before and after the removal of the Si_3N_4/SiO_2 mask, respectively. From the shift of the envelope maxima for the wire samples (Fig. 5 (b) and (c)) with respect to the substrate peak (a), the mean in-plane strain $\langle\varepsilon_{xx}\rangle$ is obtained to be $\langle\varepsilon_{xx,a}\rangle = 4.8\times10^{-4}$ and $\langle\varepsilon_{xx,b}\rangle = 7.5\times10^{-4}$, respectively. Apparently, after removing the SiO_2/Si_3N_4 mask (Fig.5 (c)) the in-plane lattice relaxation of the SiGe/Si wire structure becomes *larger*.

In order to explain these observations, finite element (FEM) calculations were performed to describe the inhomogeneous strain distribution present in the wires. The calculated results (Fig. 6 (a), (b)) clearly show that the strain distribution is very inhomogeneous. In $Si_{1-x}Ge_x$ MQW layers the maximum strain relaxation occurs close to the edge of the wires. The in-plane strain is larger at the top of the wires than it is at the bottom, reflecting the larger relaxation at the top. The strain extending into the Si substrate has both tensile and compressive components. The presence of the SiO_2 mask causes a tensile force to the substrate, which reduces the in-plane lattice relaxation in the SiGe wires (Fig. 6 (a)) . Removing the SiO_2 mask (Fig. 6 (b)), the tensile force disappears, leading to further elastic lattice relaxation in the substrate and consequently to an enhancement of the relaxation in the Si/SiGe wires.

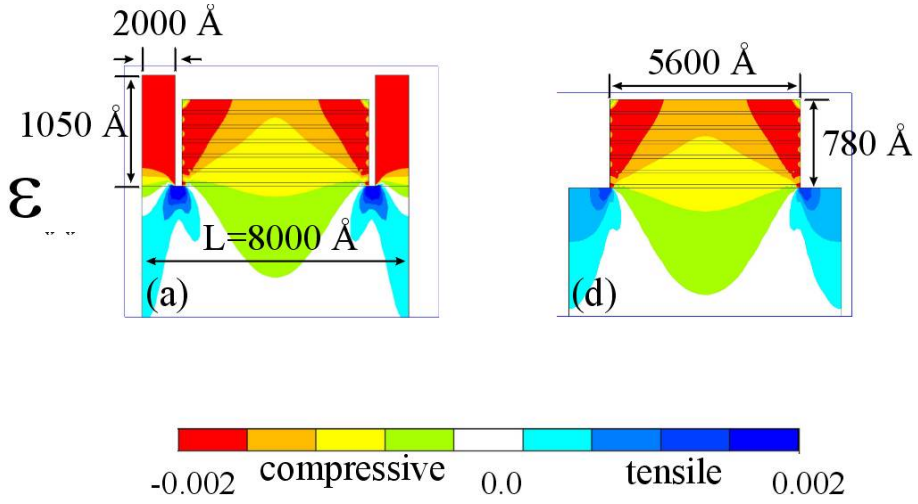

Fig. 6: Contour plots of strain tensor component ε_{xx} obtained from finite element calculations for a Si/SiGe wire sample (Fig.1b) with the mask (a) and after removal of the shadow mask (b).

3. Conclusion

SiGe quantum wells with finite lateral size grown by solid source MBE, using three different kinds of masks, were investigated with respect to their structural and optical properties. It turns out that the luminescence efficiency of wires grown into deep etched Si is much higher compared to those grown with oxide masks alone. This is due to the fact that defects at the interfaces are avoided. Detailed investigations of the lattice strain were performed both experimentally using x-ray diffraction techniques and theoretically

by finite element calculations. The in-plane lattice strains are depth dependent and change after the patterned mask layer is removed.

Acknowledgements

This work was supported by ÖAD (Y.Zh.), and by the FWF.

References

[1] T. Köster, J. Gondermann, B. Hadam, B. Spangenberg, M. Schütze, H. G. Roskos, and H. Kurz, *J. Vac. Sci. Technol.* B 14 (1996) 698.

[2] S.C. Jain, H.E. Maes, K. Pinardi, *Thin Solid Films* 292 (1997) 218.

[2] J. Brunner, T. S. Rupp, H. Gossner, R. Ritter, I. Eisele, and G. Abstreiter, *Appl. Phys. Lett.* 64 (1994) 994.

[3] J. Brunner, P. Schittenhelm, J. Gonderman, B. Spangenberg, B. Hadam, T. Köster, H. G. Roskos, H. Kurz, H. Gossner, I. Eisele, and G. Abstreiter, *J. Cryst. Growth* 150 (1995) 1060.

[4] M. Kim, H. J. Osten, A. Wolff, C. Quick, H. P. Zeindl, J. Klatt, and D. Knoll, *J. Cryst. Growth* 167 (1996) 508.

[5] E. S. Kim, N. Usami, and Y. Shiraki, *Appl. Phys. Lett.* 72 (1998) 1617.

[6] H. Hirayama, T. Tatsumi, N. Aizaki, *Appl.Phys. Lett.* 52 (1998) 2242.

[7] Y. Zhuang, V. Holy, J. Stangl, A. A. Darhuber, P. Mikulik, S. Zerlauth, F. Schäffler, G. Bauer, N. Darowski, D. Lübbert, and U. Pietsch, J. Phys. D: Appl. Phys. 32 (1999) A224; Y.Zhuang et al. *Journal of Materials Science: Materials in Electronics* 10 (1999) 215.

[8] M. E. Keeffe, C. C. Umbach, and J. M. Blakely, *J. Phys. Chem. Solids* 55 (1994) 965.

[9] Z. L. Liau, and H. J. Zeiger, *J. Appl. Phys.* 67 (1990) 2434.

[10] M. Ozdemir, and A. Zangwill, *J. Vac. Sci. Technol.* A 10 (1992) 684.

[11] N. Darowski, K. Paschke, U. Pietsch, K. Wang, A. Forchel, D. Lübbert and T. Baumbach, *Physica* B 248 (1998) 104.